Acta Crystallographica Section A
Foundations of Crystallography
ISSN 0108-7673

Received 8 March 2004
Accepted 14 July 2004

© 2004 International Union of Crystallography
Printed in Great Britain – all rights reserved

Extinction-free electron diffraction refinement of bonding in $SrTiO_3$

Jesper Friis,[a]* Bin Jiang,[b] John Spence,[b] Knut Marthinsen[c] and Randi Holmestad[a]

[a]Department of Physics, Norwegian University of Science and Technology (NTNU), N-7491 Trondheim, Norway, [b]Department of Physics and Astronomy, Arizona State University, Tempe, AZ 85287-1504, USA, and [c]Department of Materials Technology, Norwegian University of Science and Technology (NTNU), N-7491 Trondheim, Norway. Correspondence e-mail: jesper.friis@material.ntnu.no

Accurate low-order Fourier coefficients of the crystal potential of $SrTiO_3$ are measured by quantitative convergent-beam electron diffraction. The accuracy in the corresponding derived X-ray structure factors is about 0.1% for the strong low-order reflections ($\sin\theta/\lambda < 0.3$ Å^{-1}). This accuracy is better than for conventional X-ray diffraction and equivalent to the accuracy of the X-ray *Pendellösung* method. Combination of these structure factors with high-order X-ray diffraction measurements allows accurate bonding information to be obtained from a multipole model fitted to the experimental data. It is shown that Ti—O has a covalent component and that the Sr—O bond is mainly ionic. The role of Ti 3*d* electrons in Ti—O bonding is also discussed.

1. Introduction

Strontium titanate ($SrTiO_3$) is a typical perovskite structure, with incipient ferroelectric properties at ambient temperature and a displacive phase transition from a cubic to a tetragonal structure at around 106 K. The cubic phase structure of $SrTiO_3$ is shown schematically in Fig. 1. The covalent component of the chemical bonding in perovskites is considered important for understanding their physical properties, such as incipient ferroelectricity. Theoretical calculations using density functional theory (DFT) show that the Ti—O bonding is polar covalent, while the Sr—O bonding has mainly ionic character (Weyrich & Siems, 1985). Despite being quantitatively very different, the experimental deformation density maps of Buttner & Maslen, (1992) and Abramov *et al.* (1995) show a charge accumulation in the Ti—O bonds. Similar results were also obtained by X-ray powder diffraction experiments analyzed with the maximum-entropy method (Ikeda *et al.*, 1998). A more detailed quantitative characterization of the charge density was performed by Zhurova & Tsirelson (2002), based on a multipole analysis of X-ray experiments at 145 K (Abramov *et al.*, 1995).

It is well known that low-order structure factors contain significant information on the valence-charge distribution (Zuo *et al.*, 2000), important for chemical bonding. Fig. 2 shows the valence scattering in $SrTiO_3$ from the Sr, Ti and O atoms. There are only three reflections contributing to the valence scattering of Sr ($\sin\theta/\lambda < 0.25$ Å^{-1}) and 14 contributing to the valence scattering of Ti ($\sin\theta/\lambda < 0.5$ Å^{-1}). Unfortunately, most of these reflections are strong ($Q > 1.30$ m^{-1}, see Table 1) and therefore strongly affected by extinction. This makes multipole refinements based on X-ray diffraction difficult. In the present work, we overcome this problem by measuring the structure factors affected by

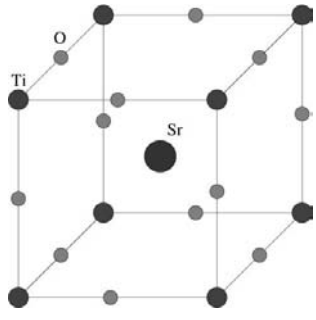

Figure 1
Schematic drawing of the unit cell of $SrTiO_3$ in the cubic phase. The Sr and Ti atoms are at cubic site-symmetry positions $m\bar{3}m$, while the O atoms have the site symmetry $4/mmm$.

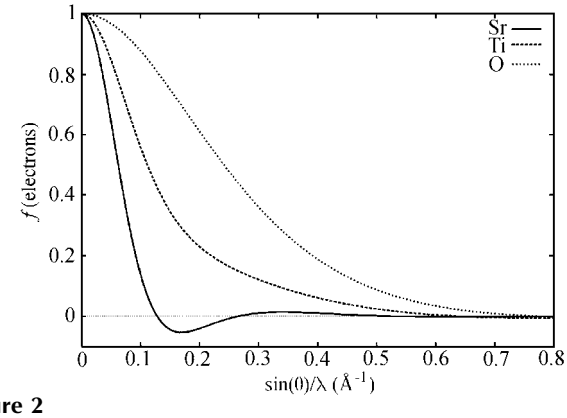

Figure 2
Valence-electron scattering factors of Sr($4s^2$), Ti($3d^2 4s^2$) and O($2s^2 2p^4$) atoms. Note: all scattering factors are normalized to one.

Table 1
Experimental and theoretical static lattice structure factors for the cubic phase of $SrTiO_3$.

Q is the scattering strength for the X-ray data, defined as $Q = [|(e^2F)/(4\pi\varepsilon_0 m_e c^2 V)|^2][\lambda^3/\sin(2\theta)]$ (in units of m^{-1}), where λ is the wavelength, θ the diffraction angle, F the X-ray structure factor and V the volume of the unit cell. n is the number of independent QCBED refinements performed in order to obtain the electron structure factors $U_{\mathbf{g}}$ and absorption U'_g. The IAM values are calculated from Su & Coppens (1997) and the DFT values with *WIEN2k* (Blaha *et al.*, 2001) using the generalized gradient approximation (Perdew *et al.*, 1996). The X-ray data are from Abramov *et al.* (1995).

hkl	$\sin\theta/\lambda$ (Å^{-1})	Q	n	U_g	U'_g	IAM	DFT	X-ray	This experiment
100	0.128	0.247	4	0.0012 (2)	0.0008 (2)	7.89	7.80	7.85 (5)	7.88 (2)
110	0.181	4.748	5	0.0527 (2)	0.0020 (2)	42.48	41.06	40.64 (10)	40.93 (4)
200	0.256	6.412	8	0.0649 (2)	0.0023 (2)	56.13	56.51	56.92 (14)	56.53 (6)
220	0.363	2.980	5	0.0437 (5)	0.0024 (2)	45.39	45.41	45.05 (11)	45.42 (13)
111	0.222	2.131	3	0.0303 (1)	0.00100 (3)	29.43	30.38	30.63 (10)	30.40 (4)
211	0.314	1.928	5	0.0281 (1)	0.0018 (1)	34.27	34.14	33.95 (8)	34.15 (7)
222	0.444	1.856	3	0.03387 (6)	0.00160 (4)	39.31	39.31	38.88 (10)	39.27 (7)
400	0.513	1.338	4	0.02711 (6)	0.0016 (1)	35.39	35.52	35.07 (10)	35.34 (11)
310	0.405	1.196	3	0.0203 (2)	0.0007 (5)	30.13	30.30	30.26 (7)	30.09 (16)
321	0.480	0.844	4	0.0162 (2)	0.0012 (1)	27.34	27.42	27.36 (6)	27.35 (20)
422	0.628	0.840	4	0.01914 (8)	0.0012 (1)	30.49	30.54	30.43 (7)	30.60 (40)
311	0.425	0.488	4	0.0164 (2)	0.0009 (1)	19.84	19.77	19.73 (5)	19.89 (17)

extinction with convergent-beam electron diffraction (CBED), which allows very accurate absolute scale measurements of absorption and extinction-free low-order structure factors (Spence & Zuo, 1992). This technique can be seen as a complement to X-ray diffraction and a combination of the two methods has been shown to be very successful (Zuo *et al.*, 1999; Friis, Madsen *et al.*, 2003).

In the CBED technique, the electron beam in a transmission electron microscope (TEM) is focused to a probe a few nanometres in diameter on a crystal of thickness 500 to 1000 Å. Using the image mode of the TEM, a perfect crystalline sample can be selected for the experiment. This allows us to compare the experimental intensities with many-beam Bloch-wave calculations of the diffraction process, and hence account for primary extinction (multiple scattering) and absorption (Zuo, 1999).

§2 presents the details on the CBED experiments and the structure-factor refinements. In §3 and §4, we present the multipole refinements and density functional theory calculations, while §5 contains the results and discussion.

2. Convergent-beam electron diffraction

2.1. Experiment

Pure colorless $SrTiO_3$ single crystals were used for the TEM sample preparation following standard preparation procedures, such as polishing, dimpling and ion-beam thinning. The samples were cleaned in a plasma cleaner before the experiments in order to reduce surface contamination. No damaged surface layer that could be introduced by the ion beam thinning process (Jiang, Zuo, Friis & Spence, 2003; Jiang, Zuo, Jiang *et al.*, 2003) was observed.

A LEO 912B transmission electron microscope, operating at 120 kV and equipped with an in-column Ω filter was used for the experiments. Energy filtering is very important, since inelastically scattered electrons are generally not included in the Bloch-wave calculations (Marthinsen *et al.*, 1994). The CBED patterns were recorded on a Gatan 1K × 1K MSC CCD camera with 14 bit dynamic range. With a double-tilt liquid-nitrogen sample holder, the temperature was kept just above the phase transition at 106 K.

Readout temperatures from the holder varied from 108 to 113 K, but we know from experience (Friis, Jiang, Spence & Holmestad, 2003) that the true sample temperature is some degrees higher, since the temperature sensor is not in direct contact with the specimen due to the limited space inside the microscope. Before further analysis, the CBED patterns were deconvoluted with the *LUCY* algorithm (Zuo, 1998) in order to compensate for point spreading in the CCD.

2.2. The refinement procedure

The electron structure factors (Fourier coefficients of the crystal potential) are determined through a refinement procedure. In short, structural and experimental parameters (such as electron structure factors, absorption, sample thickness, beam direction *etc.*) are adjusted in a Bloch-wave simulation until a perfect match is obtained between theory and experiment. The acceleration voltage of the microscope and the crystal lattice parameters need to be known accurately in advance. Since the effects of these two parameters are highly correlated, they have to be determined separately. The acceleration voltage was calibrated to be 119.60 (1) keV using a standard silicon crystal (Friis, Jiang, Spence & Holmestad, 2003).

2.3. Lattice-parameter determination

Even though there have been many measurements of the lattice parameters in $SrTiO_3$ (Lytle, 1964; Abramov *et al.*, 1995), these values are difficult to use since the exact experimental temperature is unknown. However, by using the exact position of the high-order Laue-zone (HOLZ) lines, it is possible to measure the lattice parameter very accurately directly from a CBED pattern (Zuo *et al.*, 1998).

Fig. 3(*a*) shows a CBED pattern of the center disc close to the [014] zone axis. Dynamical calculations of the exact HOLZ-line positions were performed in the three areas

marked in the figure. These areas contain HOLZ-line crossings sensitive to the lattice parameter and are chosen to limit the influence of low-order structure factors that might be affected by bonding and hence differ from their independent-atom-model (IAM) values. Since only the HOLZ-line positions are of interest, the CBED pattern was made binary using a threshold of 25% of the full image intensity (Fig. 3*b*). The refinement was performed with the *EXTAL* program (Zuo, 1998) in a two-step procedure. First, a full-intensity refinement of the experimental parameters (incident-beam angle, sample thickness and pattern geometry) was performed. These values were then used as a starting point in the lattice-parameter refinement based on the binary pattern. The lattice parameter for the best fit was $a = 3.899\ (1)$ Å.

It should be pointed out that this method for lattice-parameter refinement only considers the relative positions of HOLZ lines and is therefore not affected by the camera length of the TEM. With acceleration voltage calibrated by a silicon crystal, the accuracy is equivalent to that of X-ray diffraction using a synchrotron source (Zuo, 1998).

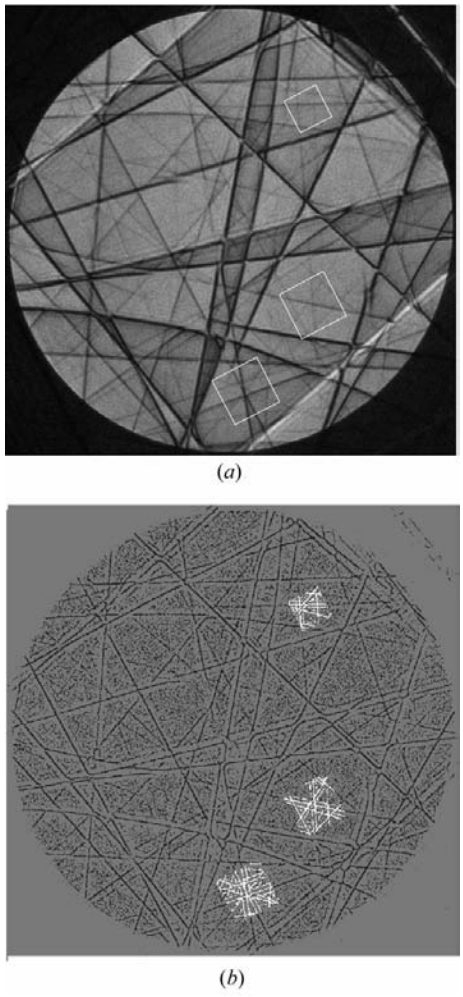

Figure 3
Determination of the lattice parameter. (*a*) CBED pattern of the central disc, close to the [014] zone axis in $SrTiO_3$. The three areas chosen for lattice-parameter refinement are shown. (*b*) Binary version of the CBED pattern in (*a*). The calculated HOLZ-line positions used in the refinement are shown with white overlay.

2.4. Structure-factor refinements

CBED patterns recorded in the systematic row diffraction orientation were used for the structure-factor refinements. An example for the (110) systematic row is shown in Fig. 4. In this orientation, the recorded intensities are highly sensitive to the (normally two or three) low-order structure factors for which the Bragg condition is satisfied. Only these (two or three) structure factors are refined. All the other structure factors included in the refinement (normally 300–400) are kept fixed at their IAM values. For the high-order structure factors, reliable values for the anisotropic displacement parameters (ADPs) are needed. These were calculated using the Debye approximation (Coppens, 1997). The sensitivity to the small errors resulting from this approximation has been minimized by choosing beam orientations with as few HOLZ lines as possible.

In order to ensure convergence of the refinement procedure, adequate starting values for the parameters to be refined must be chosen. First the sample thickness, which is a trivial but important parameter, and the incident-beam direction must be estimated. The beam direction is usually estimated by visually comparing the experimental Kikuchi-

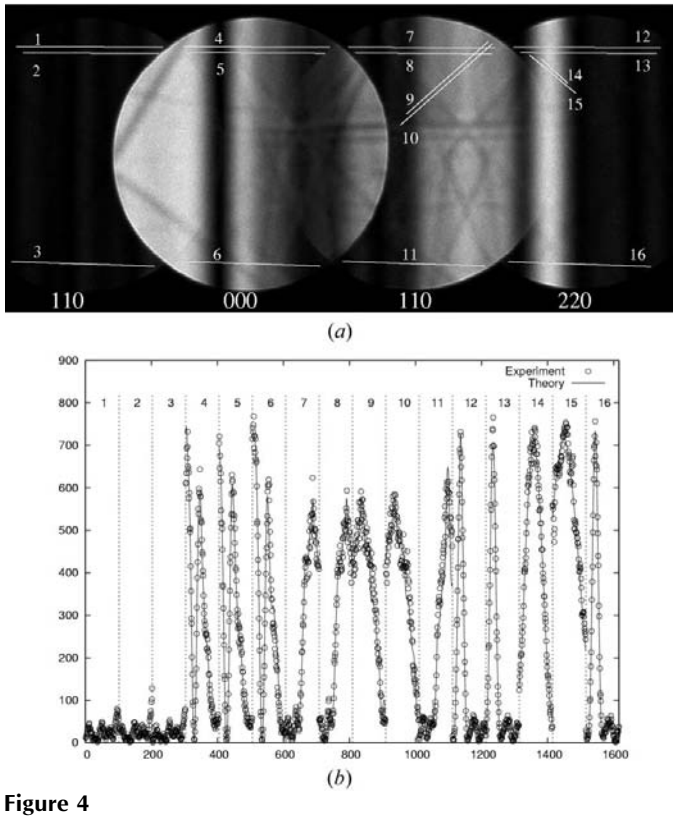

Figure 4
(*a*) CBED pattern of the (110) systematic row in $SrTiO_3$. (*b*) Best fit between theoretically calculated intensities (lines) and experiment (circles) after structure-factor refinement of the (110) systematic row shown in (*a*). For this refinement of the (110) and (220) structure factors, 1616 pixels were included along 16 line scans.

Table 2
Refined multipole parameters obtained from experiment (combination of electron and X-ray diffraction) and density functional theory.

Multipole radial functions are constructed from independent-atom radial wavefunctions (see text for details). The same multipole model is used for both data sets.

Refinement parameters	Experiment			Band theory		
	Sr	Ti	O	Sr	Ti	O
P_{00}	1.70 (4)	2.27 (1)	6.66 (5)	1.40 (4)	2.73 (1)	6.62 (3)
P_{20}			0.10 (3)			0.06 (3)
P_{40}		−0.06 (22)	0.05 (3)		0.6 (1)	−0.01 (2)
P_{44+}		$= P_{40}$	0.04 (4)		$= P_{40}$	−0.02 (2)
κ_0	0.80 (10)	1.01 (4)	0.965 (5)	1.1 (1)	1.14 (2)	0.973 (3)
κ_4		$= \kappa_0$			$= \kappa_0$	
$\alpha_3 = \alpha_4$			2.8 (3)			2.9 (4)
U^{11} ($\times 10^2$)	0.383 (1)	0.336 (2)	0.734 (9)			
U^{22} ($\times 10^2$)	$= U^{11}$	$= U^{11}$	$= U^{11}$			
U^{33} ($\times 10^2$)	$= U^{11}$	$= U^{11}$	0.293 (11)			
$R_w(\|F\|)$ (%)		0.46			0.26	

and HOLZ-line patterns with kinematic calculations (Zhu & Zuo, 1994). The structure factors are initially estimated from Doyle & Turner (1968) or DFT, and the *ATOM* subroutine of Bird & King (1990) is used to estimate the absorption part.[1]

In total thirty-two CBED patterns of seven different systematic rows were used in the refinement of the twelve structure factors given in Table 1. In order to ensure consistency, the CBED patterns were recorded at different specimen thicknesses, ranging from 500 to 1000 Å, and with different beam orientations. The structure factors and their corresponding standard deviations, listed in Table 1, are obtained from the individual measurements $U_{\mathbf{g}i}$, by

$$U_{\mathbf{g}} = \sum_i w_{\mathbf{g}i} U_{\mathbf{g}i} \tag{1}$$

and

$$\sigma^2(U_{\mathbf{g}}) = \sum_i w_{\mathbf{g}i}^2 s_{\mathbf{g}i}^2 + \sum_i w_{\mathbf{g}i}^2 (U_{\mathbf{g}i} - U_{\mathbf{g}})^2, \tag{2}$$

where $s_{\mathbf{g}i}$ is the estimated standard deviation of refinement i and the weights $w_{\mathbf{g}i}$ are $(1/s_{\mathbf{g}i})/(\sum_j 1/s_{\mathbf{g}j})$.

These electron structure factors were converted to X-ray structure factors (Fourier coefficients of the electron density) through the reciprocal version of Poisson's equation, known as the Mott formula (Spence & Zuo, 1992).

3. Multipole modeling

We based our multipole refinement on the 131 structure factors measured by Abramov *et al.* (1995) using Mo $K\alpha$ X-radiation at 145 K. Eight of the low-order reflections prone to extinction were replaced by our CBED measurements converted to 145 K (using the Debye approximation; Coppens, 1997). The errors introduced by this conversion are very small, since only low-order structure factors were converted.

[1] Absorption is treated as a complex component U' of the electron structure factor U. It accounts mainly for thermal diffuse scattered electrons that cannot be removed by the energy filter.

The refinement of the original X-ray data (Abramov *et al.*, 1995) shows anharmonic ADPs that were confirmed in the reanalysis (Zhurova & Tsirelson 2002). However, other experiments [neutron diffraction at 112 K (Hutton *et al.*, 1981), γ-ray diffraction at 111 K (Jauch & Palmer, 1999) and synchrotron X-ray diffraction at 130, 300 and 873 K (Kiat *et al.*, 2000)] show no anharmonicity in $SrTiO_3$. Here we have therefore performed the multipole refinement both with and without anharmonicity.

Because of their cubic site symmetry, Sr and Ti atoms have only one harmonic component U^{11} while the O atom has two, U^{11} and U^{33}. When including anharmonicity, all third-order coefficients in the Gram–Charlier expansion vanish because of centrosymmetry. Sr and Ti atoms each have two fourth-order coefficients, D^{1111} and D^{1122}, while the O atom has three, D^{1111}, D^{2222} and D^{1122} (Johnson & Levy, 1974), resulting in seven additional parameters to refine when including anharmonicity.

In the multipole model, 12 additional parameters were refined, including electron populations in valence orbitals (monopoles), multipoles up to fourth order and corresponding radial expansion (κ) parameters (see Table 2). The allowed multipoles were selected according to the index-picking rules of Kurki-Suonio (1977). The Sr atom was treated as spherical, since initial refinements showed very small non-spherical charge deformation of the Sr atom.

The multipole refinements were performed with the *VALRAY* program (Stewart *et al.*, 2000) using different scattering tables. The best fit was obtained using the relativistic multiconfiguration Dirac–Fock scattering factors by Macchi & Coppens (2001) for Sr atoms and similar calculations by Su & Coppens (1998) for Ti and O atoms. On the other hand, the non-relativistic Hartree–Fock calculation of Clementi & Roetti, (1974) resulted in poor fits and large κ values. The charge deformation maps (Figs. 5*a*, *b*) were calculated using the refined multipole parameters in direct space. Charge deformation maps were obtained by subtracting the charge density of the spherical IAM model from our measured densities.

4. Density functional theory

Band-theory calculations, based on DFT, were performed using the full-potential linearized augmented plane-wave + local orbitals method (LAPW + lo) (Sjöstedt *et al.*, 2000) as implemented in *WIEN2k* (Blaha *et al.*, 2001). Exchange and correlation effects were treated within density functional theory, using the generalized gradient approximation (GGA) (Perdew *et al.*, 1996). Core electrons were treated fully relativistically and valence electrons scalar relativistically. The modified tetrahedron method was used for Brillouin-zone integration (Blöchl *et al.*, 1994). The **k**-point convergence was tested using a total of 10000 **k** points in the unit cell with

$R_{mt} \times \mathbf{k}_{max}$ equal to 8.0. Muffin-tin radii of 2.0 a.u. for the Sr atom and 1.7 a.u. for Ti and O atoms were used with a basis-set size of 769 (36 local orbitals).

5. Results and discussion

Fig. 6 shows the structure factors obtained from CBED, X-ray diffraction, DFT and multipole refinement. Some significant differences between CBED and X-ray diffraction can be seen for the strongest low-order reflections. However, it is interesting to notice that for the weak 100 reflection, for which extinction effects should be small, the agreement between X-ray and CBED is within one standard deviation. Our suggestion, that these differences are due to extinction problems for X-ray diffraction, is corroborated by the in general better agreement between DFT and CBED.

In order to illustrate the accuracy of CBED compared to X-ray diffraction, we have included the scattering strength Q in Table 1. According to the Zachariasen model (Zachariasen, 1967), the extinction correction is given by $y_p = 1/(1 + 4/3Qt\alpha)^{1/2}$. The larger Q, the stronger is the extinction effect in X-ray diffraction. It is noticed that, for the strong low-order reflections with $Q \geq 1.8\ \mathrm{m}^{-1}$, the accuracy of the electron diffraction measurements are superior to that of X-ray diffraction. A mutipole refinement based on the original X-ray data set (not included in the paper) also showed decreased consistency between the fitted and measured strong low-order structure factors. Thus, more accurate bonding features can be discovered using CBED.

The results from the multipole refinement including only harmonic ADPs are shown in Table 2. By including anharmonicity, which adds seven extra variables to the refinement, the residual is only slightly reduced from 0.46 to 0.41%, but a lot of correlation between the ADPs are at the same time introduced. This suggests that $SrTiO_3$ is not affected by anharmonicity at 145 K and this is in excellent agreement with several other experiments (Hutton *et al.*, 1981; Jauch & Palmer, 1999; Kiat *et al.*, 2000).

In order to test the multipole model, the deformation densities are compared directly to DFT (Figs. 5*c*, *d*) and a multipole refinement of theoretical structure factors from DFT (Figs. 5*e*, *f*). The DFT calculations show a small nearly spherical charge deficiency near the Sr atom (less than -0.02 e Å^{-3}), indicating weak ionic Sr—O bonding. It also shows a charge transfer from Ti to O atom and charge accumulation in the Ti—O bond with peak value of 0.2 e Å^{-3}, suggesting polar covalent Ti—O bonding. The multipole model based on DFT (Figs. 5*e*, *f*) qualitatively reproduces these bonding features. The largest difference is that the Ti—O bonding peak is moved closer to the O atom and the peak value is increased to 0.3 e Å^{-3}. We can therefore conclude that our multipole model is able to reproduce bonding details but the differences also demonstrate the shortcomings of the multipole model, where independent-atom valence-orbital wavefunctions are used as valence wavefunctions in the κ formalism (Stewart *et al.*, 2000).

Table 2 shows small differences between the refined multipole parameters obtained from experimental and theor-

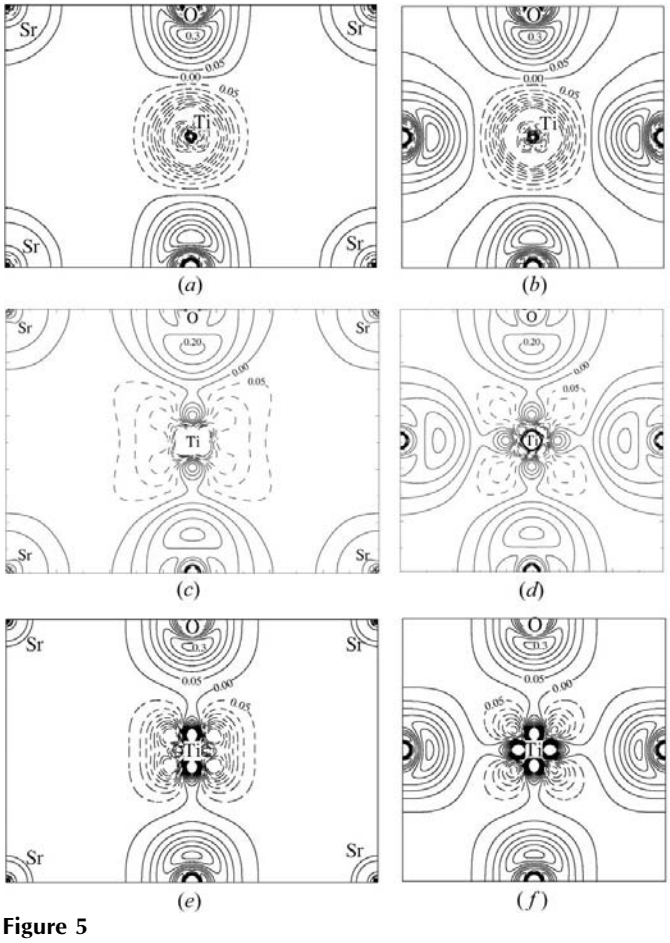

Figure 5
Experimental and theoretical deformation-density maps for $SrTiO_3$ of the (110) (left) and (100) (right) planes passing through the Ti atoms. (*a*), (*b*) Multipole refinement of experimental structure factors; (*c*), (*d*) density functional theory (DFT); (*e*), (*f*) multipole refinements of theoretical structure factors from DFT. Dashed contours are for $\Delta\rho < 0$ and solid contours are for $\Delta\rho \geq 0$. The contour values range from -0.4 to 0.4 e Å^{-3} with an increment of 0.05 e Å^{-3}.

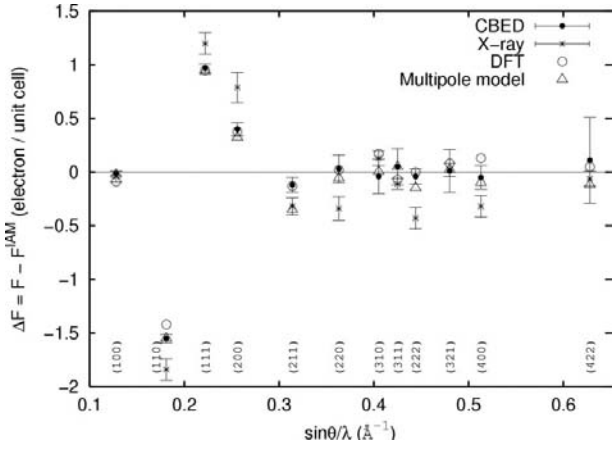

Figure 6
Difference between the independent-atom model and structure factors from CBED, X-ray diffraction, DFT and the multipole model based on experiment plotted *versus* scattering angle.

etical structure factors. The largest difference is the cubic hexadecapole population of Ti, which is responsible for the diagonal lobes of charge depletion seen in Fig. 5(*f*), but not in Fig. 5(*b*).

The experimentally based charge deformation maps (Figs. 5*a*, *b*) are very similar to the theoretical ones (Fig. 5*e*, *f*). They show spherical charge deformation at Sr-atom positions (expected since the model does not include asphericity for Sr atoms), weak ionic Sr—O bonding and polar covalent Ti—O bonding. The Ti—O bonding peaks are at the same position and have similar strength (0.3 e Å^{-3}).

Error analysis can help determine which features in the experimental charge-density maps are reliable. Both residual and variance maps are calculated. A variance map gives the noise level, which for most of the area is less than 0.02 e Å^{-3}, except for the nuclear regions (within 0.5 Å in radius). Since also the residual map (Fig. 7) looks featureless, we consider the experimental deformation density as reliable.

The 3*d*-orbital populations for Ti show the role of the 3*d* electrons in Ti—O bonding. For Ti, with site symmetry $m\bar{3}m$, a 5×5 matrix was used to convert the multipole populations to the five canonical *d*-orbital population of t_{2g} (composed of d_{xy}, d_{xz} and d_{yz}) and e_g (composed of d_{z^2} and $d_{x^2-y^2}$) orbitals (Coppens, 1997), listed in Table 3. The total Ti valence population (monopole) is 2.57 e. To obtain the individual *d*-orbital occupancies, we assume zero occupancy of the Ti 4*s* and 4*p* orbitals. There is a indication that the two e_g orbitals, which have slightly more electrons, hybridize with the O 2*sp* orbitals to form strong Ti—O σ bonds. The three t_{2g} orbitals hybridize with O 2*sp* to form weak Ti—O π bonds.

The density of states calculated from DFT for Ti and O atoms (Fig. 8) shows two main features: (i) the bands between −5 and 0 eV are mainly from O 2*p* orbitals, indicating charge transfer from Ti to O; (ii) band hybridization occurs mainly at the bottom of the valence band for Ti 3*d* and O 2*p* valence electrons, representing covalency (at the top of the valence band we find mostly non-bonding O 2*p* electrons). These calculations agree well with the experimental result that the Ti—O bonding is polar covalent.

Bonding mainly modifies the crystal valence-electron distribution and therefore only affects reflections at low scattering angles. Fig. 6 shows that, for $SrTiO_3$, only structure factors up to $\sin\theta/\lambda \leq 0.3$ Å^{-1} differ significantly from the independent-atom model. These reflections are measured very accurately with CBED. It is also seen that DFT agrees very well with the CBED measurements, except for the two lowest-order reflections, 100 and 110. This difference is significant and exposes approximations made in the DFT functional. In this work, we have used the GGA functional of Perdew *et al.*, (1996), which is generally accepted as very accurate. However, for Mg, it has been shown (Friis, Madsen *et al.*, 2003) that a more accurate description of the valence density can be obtained by the local density approximation (exact for a free-electron gas) including the self-interaction correction of Lundin & Eriksson (2001).

Table 3
The calculated Ti-atom 3*d* orbital populations from multipole parameters in Table 2.

Note: we assume zero occupancy for 4*s* and 4*p* orbitals.

	Orbital	Orbital population (e)
t_{2g}	d_{xy}	0.47 (7)
	d_{xz}	0.47 (5)
	d_{yz}	0.47 (5)
e_g	d_{z^2}	0.43 (7)
	$d_{x^2-y^2}$	0.43 (7)
Total electron population		2.27 (1)

6. Conclusions

Accurate low-order electron structure factors of $SrTiO_3$ have been measured with CBED. These structure factors were combined with X-ray measurements in a multipole analysis, then the obtained charge deformation density was compared to deformation densities from both DFT and a multipole analysis based on DFT. From this, the Ti—O bond is found to be polar-covalent, while the Sr—O bond is weakly ionic.

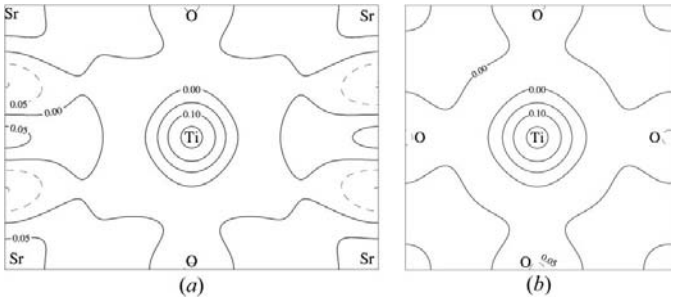

Figure 7
Residual maps of the (110) (*a*) and (100) (*b*) planes of $SrTiO_3$ passing through the Ti atoms. The contour levels are 0.05 e Å^{-3}. Dashed contours are for $\Delta\rho < 0$ and solid contours are for $\Delta\rho \geq 0$. The largest variation is ±0.05 e Å^{-3}. Errors are less than 0.01 e Å^{-3} in the interstitial region, except at high-symmetry points (featureless maps).

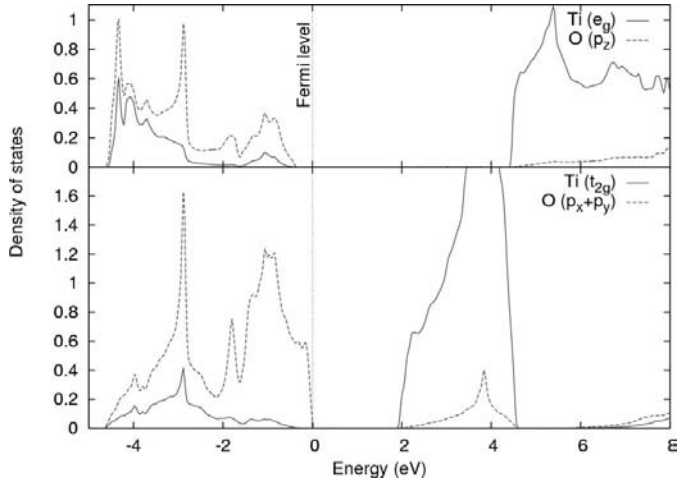

Figure 8
Decomposition of Ti and O in $SrTiO_3$ density of states into symmetry-projected Ti e_g + O p_z and Ti t_{2g} + O (p_x + p_y) contributions. For the O atom, the *z* axis is chosen in the direction of the nearest Ti atom.

Charge transfer from Ti to O atoms and orbital hybridization of Ti 3*d* and O 2*p* at the bottom of the valence band are two factors that contribute to the Ti—O bonding.

The Norwegian Research council is gratefully acknowledged for financial support through project 135270/410 and the NorLight project Heat Treatment Fundamentals (143877/213). BJ acknowledges the funding from DOE DE-FG03-02ER45596.

References

Abramov, Y. A., Tsirelson, V. G., Zavodnik, V. E., Ivanov, S. A. & Brown, I. D. (1995). *Acta Cryst.* B**51**, 942–951.

Bird, D. M. & King, Q. A. (1990). *Acta Cryst.* A**46**, 202–208.

Blaha, P., Schwarz, K., Madsen, G., Kvasnicka, D. & Luitz, J., (2001). *WIEN2k, An Augmented Plane Wave Plus Local Orbitals Program for Calculating Crystal Properties.* Vienna University of Technology, Austria.

Blöchl, P. E., Jepson, O. & Andersen, O. K. (1994). *Phys. Rev. B*, **49**, 16223–16233.

Buttner, R. H. & Maslen, E. N. (1992). *Acta Cryst.* B**48**, 639–644.

Clementi, E. & Roetti, C. (1974). *At. Data Nucl. Data Tables*, **14**, 177–478.

Coppens, P. (1997). *X-ray Charge Densities and Chemical Bonding.* Oxford University Press.

Doyle, P. A. & Turner, P. S. (1968). *Acta Cryst.* A**24**, 390–397.

Friis, J., Jiang, B., Spence, J. C. H. & Holmestad, R. (2003). *Microsc. Microanal.* **9**, 379–389.

Friis, J., Madsen, G. K. H., Larsen, F. K., Jiang, B., Marthinsen, K. & Holmestad, R. (2003). *J. Chem. Phys.* **119**, 11359–11366.

Hutton, J., Nelmes, R. J. & Scheel, H. J. (1981). *Acta Cryst.* A**37**, 916–920.

Ikeda, T., Kobayashi, T., Takata, M., Takayama, T. & Sakata, M. (1998). *Solid State Ionics*, **108**, 151–157.

Jauch, W. & Palmer, A. (1999). *Phys. Rev. B*, **60**, 0163–1829.

Jiang, B., Zuo, J. M., Friis, J. & Spence, J. C. H. (2003). *Microsc. Microanal.* **9**, 457–467.

Jiang, B., Zuo, J. M., Jiang, N., O'Keeffe, M. & Spence, J. C. H. (2003). *Acta Cryst.* A**59**, 341–350.

Johnson, C. K. & Levy, H. A. (1974). *International Tables for X-ray Crystallography*, Vol. IV, pp. 312–336. Birmingham: Kynoch Press.

Kiat, J. M., Baldinozzi, G., Dunlop, M., Malibert, C., Dkhil, B., Ménoret, C., Masson, O. & Fernandez-Diaz, M. T. (2000). *J. Phys. Condens. Matter*, **12**, 8411–8425.

Kurki-Suonio, K. (1977). *Isr. J. Chem.* **16**, 115–123.

Lundin, U. & Eriksson, O. (2001). *Int. J. Quantum Chem*. **81**, 247–252.

Lytle, F. W. (1964). *J. Appl. Phys.* **35**, 2212–2215.

Macchi, P. & Coppens, P. (2001). *Acta Cryst.* A**57**, 656–662.

Marthinsen, K., Holmestad, R. & Høier, R. (1994). *Ultramicroscopy*, **55**, 268–275.

Perdew, J. P., Burke, K. & Ernzerhof, M. (1996). *Phys. Rev. Lett.* **77**, 3865–3868.

Sjöstedt, E., Nordström, L. & Singh, D. J. (2000). *Solid State Commun.* **114**, 15–20.

Spence, J. C. H. & Zuo, J. M. (1992). *Electron Microdiffraction.* New York: Plenum Press.

Stewart, R. F., Spackman, M. A. & Flensburg, C. (2000). *VALRAY User's Manual.* Carnegie-Mellon University and University of Copenhagen.

Su, Z. & Coppens, P. (1997). *Acta Cryst.* A**53**, 749–762.

Su, Z. & Coppens, P. (1998). *Acta Cryst.* A**54**, 646–652.

Weyrich, K.-H. & Siems, R. (1985). *Z. Phys. B Condens. Matter*, **61**, 63–68.

Zachariasen, W. H. (1967). *Acta Cryst.* **23**, 558–564.

Zhu, S. & Zuo, J. M. (1994). *IdealMicroscope, EMLab software*, jianzuo@uiuc.edu.

Zhurova, E. A. & Tsirelson, V. G. (2002). *Acta Cryst.* B**58**, 567–575.

Zuo, J. M. (1998). *Mater. Trans. JIM*, **39**, 938–946.

Zuo, J. M. (1999). *Microsc. Res. Tech.* **46**, 220–233.

Zuo, J. M., Kim, M. & Holmestad, R. (1998). *J. Electron Microsc.* **47**, 121–127.

Zuo, J. M., Kim, M., O'Keeffe, M. & Spence, J. C. H. (1999). *Nature (London)*, **401**, 49–52.

Zuo, J. M., O'Keeffe, M., Kim, M. & Spence, J. C. H. (2000). *Angew. Chem. Int. Ed. Engl*. **39**, 3791–3794.